Geosynthetic effectiveness in stabilization – evaluation via Bender Element sensor

H. Wang & E. Tutumluer
Civil and Environmental Engineering Department, The Grainger College of Engineering, University of Illinois Urbana-Champaign, Urbana, USA

ABSTRACT: This paper describes an ongoing study where aggregate layer modulus enhancement due to geosynthetic stabilization was quantified via shear wave measurements using bender element (BE) sensor technology in both laboratory triaxial test setup and a large-scale testbed. Five different integral geogrids, two welded geogrids, one woven geogrid, one woven geotextile and one nonwoven geotextile were evaluated in repeated load triaxial testing. Some of the geosynthetics with good performance trends were also evaluated in a large-scale testbed. Both modulus enhancement and extent of geosynthetic influence zone were quantified. The results herein provide quantitative inputs to include geosynthetics into mechanistic-empirical pavement design.

1 INTRODUCTION

Mechanical stabilization of pavement base/subbase is often accomplished by using geosynthetics in these unbound aggregate layers. Given various geosynthetic products and different mechanisms involved, an appropriate and quantitative evaluation method of geosynthetic effectiveness is necessary. Several methods have been proposed to incorporate geosynthetics into soft subgrade stabilization including Steward et al. (1977) method, Giroud and Noiray (1981) method, Giroud and Han (2004a,b) and Army Corps of Engineers method (Tingle & Webster, 2003). Meanwhile, numerical simulations utilizing finite element modeling (FEM) and discrete element modeling (DEM) to study mechanical stabilization in paved roads and geogrid influence zones were available (McDowell et al., 2006, Kwon & Tutumluer, 2009). Recent efforts to quantify the geosynthetic effectiveness include determining soil-geosynthetic composite stiffness (K_{SGC}) (Zornberg et al., 2017) and small-strain modulus measurement via Bender Element (BE) shear wave transducers. BE sensor technology successfully quantified the modulus enhancement due to geosynthetics and distinguished different geosynthetics in a laboratory triaxial test setup (Byun and Tutumluer, 2017). With such validation, a field BE sensor was developed as instrumentation for full-scale studies (Kang et al., 2021).

The versatility of a BE field sensor aligns with the mechanical stabilization concept where the modulus enhancement can be measured at various distances away from an installed geosynthetic. With the use of a sublayering method, the stiffening due to geosynthetic can be incorporated into mechanistic-empirical (M-E) pavement design procedures where mechanically stabilized aggregate layer can be divided into sublayers having different moduli, i.e., higher modulus near geosynthetic and standard aggregate modulus farther away from geosynthetic's influence zone (Holtz et al., 2008; Vavrik, 2018). Byun et al. adopted the sublayering method for a numerical simulation and demonstrated the potential effect of geogrid stabilization for improving the mechanical behavior of pavement structures (Byun et al., 2023).

This paper describes an ongoing study where modulus enhancement due to geosynthetic stabilization was quantified via shear wave measurements using the BE sensor technology in both laboratory triaxial test setup and a large-scale testbed. Various geosynthetics were evaluated in triaxial tests and geosynthetics with good performance were also evaluated in the large-scale testbed with BE field sensors. The results from both experimental setups offered a comprehensive insight of geosynthetic stabilization effectiveness for mechanically stabilized aggregate layer inputs within the M-E pavement design framework.

2 AGGREGATES AND GEOSYNTHETICS

2.1 *Aggregates*

A crushed limestone aggregate, conforming to Illinois Department of Transportation (IDOT) CA 6 dense-graded aggregate band, was utilized in this study, as

shown in Figure 1. All triaxial specimens were engineered to follow this gradation to eliminate any effect of grain size distribution on shear wave propagations.

Following the standard Proctor compaction effort as per ASTM D698, the maximum dry density (MDD) and optimum moisture content (OMC) were determined as 2190 kg/m^3 and 5.9%, respectively. To better represent conditions in field construction, all aggregate specimens were compacted at OMC targeting MDD and the final achieved densities for triaxial specimens ranged from 2190 kg/m^3 to 2250 kg/m^3.

The same aggregates were utilized in large-scale testbed. For better consistency among test samples, air-dried aggregates were utilized to fill the testbed. The measured average water content was a low 0.17%, corresponding to a very dry condition. The average density achieved was 1870 kg/m^3 for large-scale testbed tests, lower than the MDD and triaxial specimen achieved densities. The relatively lower density is not unexpected given the dry conditions.

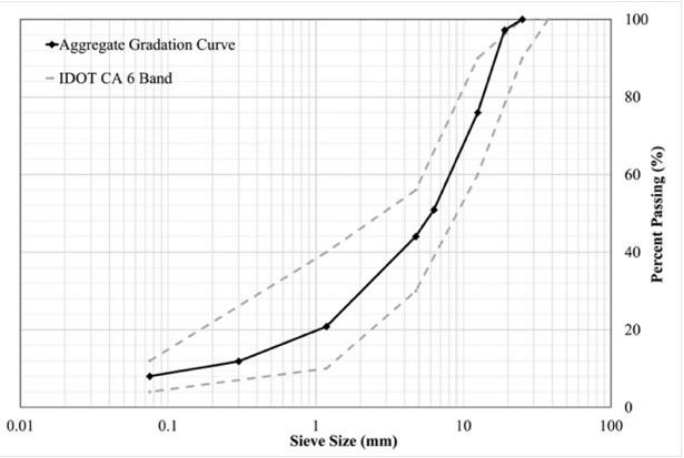

Figure 1. Aggregate gradation curve and the IDOT CA 6 band.

2.2 *Geosynthetics*

Various geosynthetics were evaluated including extruded integral geogrids (i.e., one integral geogrid with various aperture geometries, three extruded geogrids with rectangular apertures yet different rib properties, one extruded geogrid with triangular apertures), two welded geogrids with different rib strengths, one woven geogrid, one woven geotextile and one nonwoven geotextile. All geosynthetics tested herein are presented in Figure 2. Note that the photos show the individual geosynthetic coupons recovered from triaxial tests.

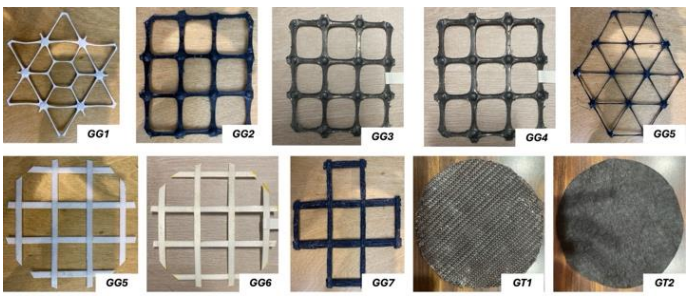

Figure 2. Geosynthetic coupons recovered from triaxial tests.

An example showing the placement of GG1 and GG4 in large-scale testbed is presented in Figure 3.

Figure 3. Geosynthetic placement in large-scale testbed.

3 EXPERIMENTAL SETUP AND METHOD

3.1 *Triaxial testing setup (TX-12)*

For laboratory triaxial tests, the TX-12 setup was utilized to conduct the repeated load resilient modulus tests. The setup can accommodate specimens with 150-mm in diameter and 300-mm height. Two internal linear variable differential transformers (LVDTs) were installed to measure axial deformations. The confining pressure was applied through compressed air inside the acrylic chamber. The load pulses were applied through a hydraulic pump and measured through a load cell at specimen top.

If placed, the geosynthetic coupons were placed at specimen midheight while for control tests, no geosynthetics were included. Three pairs of BE sensors were placed at three different heights above specimen midheight to access the modulus enhancement level at different distances from the geosynthetic. The schematic drawing of the triaxial test setup along with a photo is shown in Figure 4.

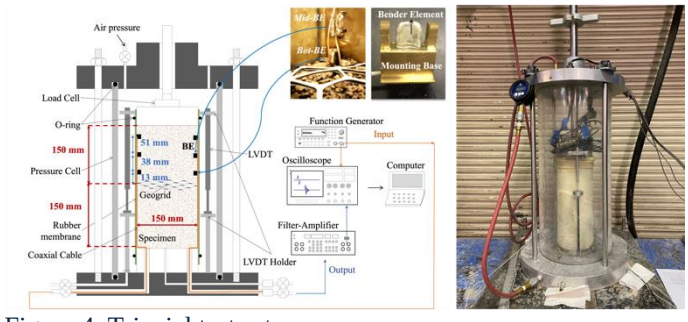

Figure 4. Triaxial test setup.

3.2 *Large-scale testbed*

A customized steel box was built to conduct the large-scale tests which is 1.83 m in length, 0.91 m in width and 0.61 m in height. A 150-mm geofoam was placed at the bottom to simulate a uniform subgrade with a California bearing ratio (CBR) value of approximately 5. On top of geofoam, a 407-mm aggregate layer was compacted in five lifts. If applicable, the geosynthetic was placed 102-mm above the geofoam.

Similarly, three pairs of BE field sensors were placed at three different heights above geosynthetic. A 229-mm diameter earth pressure cell (PC) was placed vertically above the geofoam against the steel box wall. The center of PC was 114 mm above the geofoam, which was aligned with the height of bottom BE field sensor. The schematic drawing of the large-scale testbed, photos showing the sensors and the completed test setup are presented in Figure 5. The placement of testbed on floor is deemed to have an insignicant effect on the testing herein.

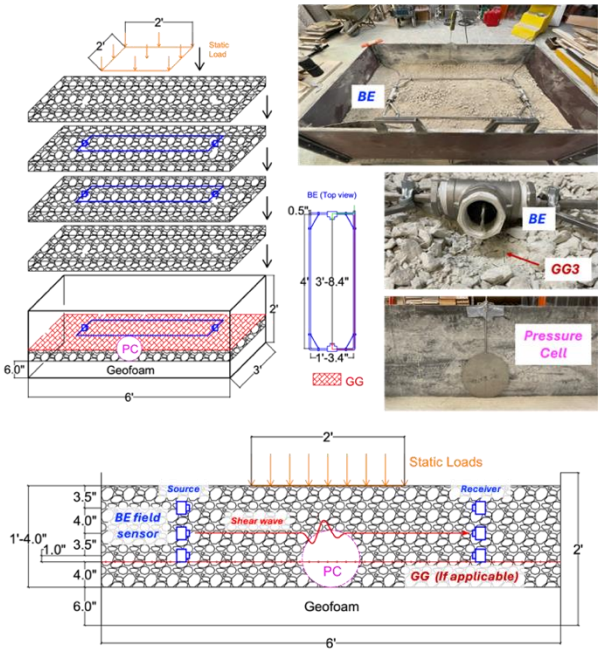

Figure 5. Large-scale testbed setup (1 ft. = 30.5 cm; 1 in. = 25.4 mm)

3.3 *Shear wave collection*

The BE sensors in both setups work as a pair with one source sensor and one receiver sensor. The source sensor was excited through a wave generator and the shear wave propagates through the aggregate media to be received by the receiver sensor. Before final collection, the received signals were filtered, amplified, stacked and averaged for a higher signal-to-noise (SNR) ratio. Compared to triaxial tests, the shear waves in large-scale testbed needed to travel a longer distance to reach receiver sensor. For this sake, a linear amplifier was used after wave generator to feed shear waves with higher amplitude into the source.

In triaxial tests, the AASHTO T 307 test procedure was followed where resilient modulus can be determined at 15 different loading stages, featuring 3 deviator stresses applied under 5 confining pressures (i.e., 20.7, 34.5, 68.9, 103.4 and 137.9 kPa) after a conditioning stage. Each loading stage consists of 100 haversine pulses. Resilient modulus was determined for each loading stage followed by the shear wave velocities measured at these confinement levels. Figure 6 shows one example of shear wave profiles collected during testing the GG5 installed specimen.

For large-scale testbed tests, a series of static loads were applied through a square steel plate placed at the center of the aggregate testbed surface. After applying each static load, shear waves were collected to assess the changes in shear wave velocities (i.e., local modulus) with loading and unloading. Similarly, the shear wave profile with GG1 collected in large-scale testbed is shown in Figure 6.

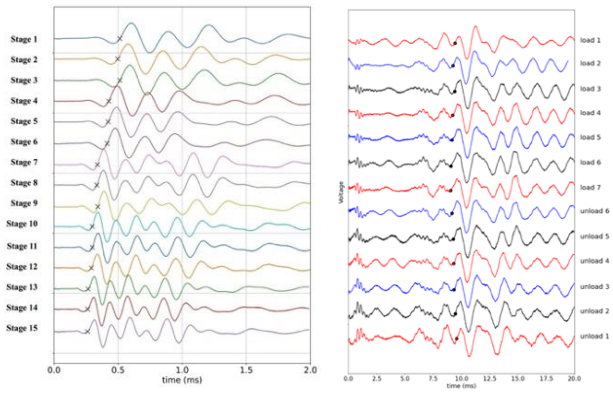

Figure 6. Shear waves collected from triaxial test (left) and large-scale testbed test (right).

4 RESULTS AND DISCUSSION

4.1 *Stiffness enhancement in triaxial tests*

Both resilient modulus and small-strain shear modulus from shear wave velocity measurements were determined in triaxial tests. Yet, the resilient modulus could not distinguish different resilient response trends among geosynthetics, as also reported by previous researchers (Abu-Farsakh et al. 2012; Byun et al. 2019). Therefore, the results for resilient modulus tests are omitted here. The small-strain shear modulus can be determined using Equation (1).

$$G_{BE} = \rho V_s^2 = \rho(L_{tip\text{-}to\text{-}tip}/t)^2 \quad (1)$$

where ρ is bulk density, V_s is shear wave velocity, $L_{tip\text{-}to\text{-}tip}$ is tip-to-tip distance between source and receiver sensor, and t is the first arrival time as highlighted with "x" symbol in Figure 6. Meanwhile, it is noted that every three signals shown in Figure 6 are similar in terms of shapes and first arrival time, which is due to the same confining pressure for every three measurements. Under the same confining pressure, although load pulses were applied in between, the specimens did not undergo significant deformation or skeleton changes, which led to similar shear wave velocities collected. Therefore, a representative G_{BE} modulus was computed at one confining pressure. The variation in G_{BE} was evaluated using the coefficient of variation (CoV), which is presented somewhere else (Wang et al., 2024). Generally, the CoV was smaller than 20%, which is considered acceptable considering the geomaterial source variation.

To evaluate geosynthetic (GS) improvement when compared to a no-geosynthetic (control) scenario, the modulus enhancement ratio for different geosynthetics is calculated using Equation (2).

Enhancement Ratio = G_{BE} with GS / G_{BE} control (2)

The enhancement ratio measured 13-mm above different geosynthetics is shown in Figure 7, which demonstrates the compatibility of different geosynthetics with dense-graded aggregates. Since there were three pairs of BE sensors installed, the influence zone of different geosynthetics can also be determined. For example, for GG1, enhancement can still be measured 51-mm above while at 102-mm above, the modulus enhancement diminished.

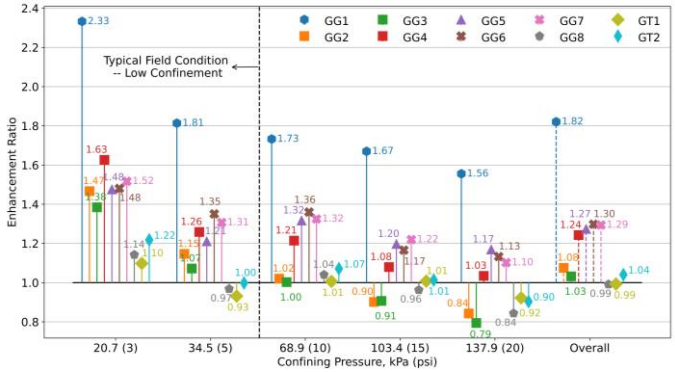

Figure 7. Enhancement ratio measured in triaxial tests.

4.2 *Stiffness enhancement in large-scale testbed*

Similarly, the enhancement and the influence zone can be quantified in large-scale testbed tests. The shear modulus profile for control and GG1 test are shown in Figure 8. Right above GG1, an average 15% modulus enhancement was achieved throughout different loading/unloading stages. While when at 142 mm above, the enhancement ratio (modulus of GG1 test compared to that of the control test) becomes 1, which indicates the GG1 influence zone as 142 mm.

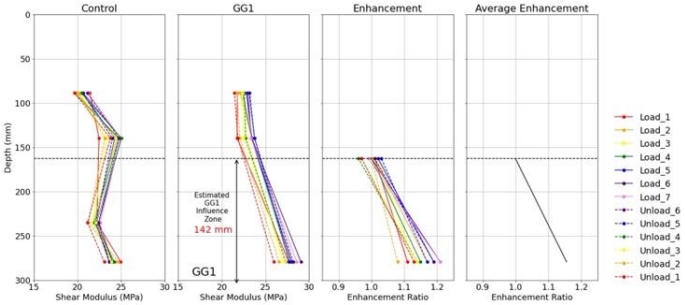

Figure 8. Geosynthetic influence zone measured in triaxial tests.

Note that given different aggregate compaction conditions and loading stages, stiffness enhancement and influence zone values from two different setups may not exactly match. Yet, the mechanically stabilized layer improvement trends agree with each other.

5 CONCLUSIONS

This paper presented results from an ongoing study aimed at investigating the effectiveness of geosynthetics in mechanical stabilization and the extent of geosynthetic influence zone using the Bender Element (BE) shear wave sensor technology in both laboratory triaxial test setup and large-scale testbed. Different geosynthetic products were evaluated with a dense-graded base course aggregate material in mechanical stabilization and for the sample modulus enhancement. The enhancement ratios and extents of geosynthetic influence zone presented herein may provide geosynthetic specific quantitative inputs into mechanistic-empirical pavement design procedures.

6 REFERENCES

Byun, Y.-H. & Tutumluer, E. 2017. Bender elements successfully quantified stiffness enhancement provided by geogrid–aggregate interlock. Transportation Research Record, 2656, 31-39.

Byun, Y.-H., Qamhia, I. I., Kang, M., Tutumluer, E. & Wayne, M. H. 2023. Modeling geogrid-stabilized aggregate base courses considering local stiffness enhancement. Geosynthetics International, 1-10.

Giroud, J. & Han, J. 2004a. Design method for geogrid-reinforced unpaved roads. II. Calibration and applications. Journal of Geotechnical and Geoenvironmental Engineering, 130, 787-797.

Giroud, J.-P. & Noiray, L. 1981. Geotextile-reinforced unpaved road design. Journal of the Geotechnical Engineering Division, 107, 1233-1254.

Giroud, J. P. & Han, J. 2004b. Design method for geogrid-reinforced unpaved roads. I. Development of design method. Journal of geotechnical and geoenvironmental engineering, 130, 775-786.

Holtz, R. D., Christopher, B. R. & Berg, R. R. 2008. Geosynthetic design & construction guidelines: reference manual. Journal.

Kang, M., Qamhia, I. I., Tutumluer, E., Hong, W.-T. & Tingle, J. S. 2021. Bender element field sensor for the measurement of pavement base and subbase stiffness characteristics. Transportation Research Record, 2675, 394-407.

Kwon, J. & Tutumluer, E. 2009. Geogrid Base Reinforcement with Aggregate Interlock and Modeling of Associated Stiffness Enhancement in Mechanistic Pavement Analysis. Transportation Research Record, 2116, 85-95.

McDowell, G. R., Harireche, O., Konietzky, H., Brown, S. F. & Thom, N. H. 2006. Discrete element modelling of geogrid-reinforced aggregates. Proceedings of the Institution of Civil Engineers - Geotechnical Engineering, 159, 35-48.

Steward, J. E., Williamson, R. & Mohney, J. 1977. Guidelines for use of fabrics in construction and maintenance of low-volume roads. Journal.

Tingle, J. S. & Webster, S. L. 2003. Corps of Engineers Design of Geosynthetic-Reinforced Unpawed Roads. Transportation research record, 1849, 193-201.

Vavrik, W. 2018. Recommended practice for incorporating geogrids in ME pavement design. Presentation at the Tensar International Congress, Roatan, Honduras, by Bill Vavrik of Applied Research Associates on July.

Wang, H., Kang, M., Kim, Y., Qamhia, I. I. A., Tutumluer, E. & Shoup, H. 2024. Geosynthetic-stabilized aggregate: quantitative modulus evaluation via bender element. Geosynthetics International, 1-13.

Zornberg, J. G., Roodi, G. H. & Gupta, R. 2017. Stiffness of soil–geosynthetic composite under small displacements: I. Model development. Journal of Geotechnical and Geoenvironmental Engineering, 143, 04017075.